Inflammation (2025) 48:4398–4413
https://doi.org/10.1007/s10753-025-02333-1

RESEARCH

miR-182-Mediated Dysregulation of Histidine Metabolism Compromises T Cell Immunity in Sepsis

Yaolu Zhang[1,2] · Jie Lian[1,2] · Lujia Zhu[1,2] · Yamei Wei[1,2] · Kaikai Wang[1,2] · Zhongqiu Lu[1,2] · Longwang Chen[1,2]

Received: 17 April 2025 / Revised: 5 June 2025 / Accepted: 12 June 2025 / Published online: 17 July 2025

Abstract

MicroRNA-182 (miR-182) exhibits immunomodulatory effects in regulating inflammatory responses to bacterial infection. However, the involvement of miR-182 in regulating T-cell immune function and differentiation in sepsis remains unknown. This study investigated the role of miR-182 in regulating T cell immune function and its mechanism in sepsis-induced immunosuppression. Using the cecum ligation and puncture model to mimic experimental sepsis, we found a significant reduction in splenic lymphocyte numbers and dysregulated T cell differentiation in septic mice. miR-182 expression was elevated in septic mice. Its knockout improved T cell immune function, ameliorated organ damage and improved survival rates in septic mice. Metabolomic and proteomic profiling revealed that histidine catabolism was attenuated and histidine was increased after miR-182 knockout. L-histidine supplementation alleviated T-cell immunosuppression in vivo. In addition, elevated plasma miR-182 levels were correlated with poor clinical prognosis in sepsis patients. Our findings demonstrate that miR-182 deficiency ameliorates the immunosuppression of T cells through the modulation of histidine metabolism, offering novel insights into the molecular mechanisms underlying T-cell dysfunction in sepsis.

Keywords Sepsis · T Cell · MicroRNA-182 · Histidine Metabolism · Immunity.

Introduction

Sepsis is a life-threatening organ dysfunction caused by a dysregulated host response to infection [1]. Sepsis and septic shock represent significant global health challenges, affecting millions annually and causing death in approximately one out of every three to six individuals diagnosed [2]. T cells are derived from hematopoietic stem cells in the bone marrow and undergo maturation in the thymus to become immunologically active lymphocytes. In sepsis, abnormal T cell differentiation and immune paralysis are characterized by reduced populations of $CD4^+$ T cells, $CD8^+$ T cells, and T helper (Th) 17 cells, coupled with an expansion of regulatory T cells (Tregs), a polarization shift from Th1 to Th2 responses, and impaired proliferative potential [3–5]. Abnormal T cell differentiation and immunosuppression are critical contributors to poor clinical outcomes in sepsis patients. However, the regulatory mechanisms of T cell differentiation remain poorly understood, and in-depth study of the regulatory mechanism of T cell differentiation and modification of T cell immune paralysis can help provide a new strategy for the immunotherapy of sepsis.

MicroRNA (miRNA) is a single-stranded non-coding RNA molecule about 22 nt long. miRNA serves as a critical link between the innate and adaptive immune system, and acts as a fine-tuner of the inflammatory response mainly through the regulation of Toll-like receptor (TLR) signaling pathways [6, 7]. Recently, it was reported that microRNA-182 (miR-182) played an important role in adaptive immune response. The IL-2-induced miR-182 inhibits Foxo1, a suppressor of proliferation expressed in resting Th lymphocytes, and contributes to the population expansion of Th cells [8]. Moreover, some studies reported that miR-182 was significantly upregulated in peripheral

Yaolu Zhang and Jie Lian contributed equally to this work.

✉ Zhongqiu Lu
lzq_640815@163.com

✉ Longwang Chen
chenlongwang1129@126.com

[1] Emergency Department, The First Affiliated Hospital of Wenzhou Medical University, Wenzhou 325000, China

[2] Wenzhou Key Laboratory of Emergency and Disaster Medicine, Wenzhou 325000, China

blood of sepsis patients [9]. Thus, we hypothesize that miR-182 regulates sepsis, particularly T cell differentiation and immune function.

Histidine is an essential amino acid that cannot be endogenously synthesized by humans. It is involved in several key processes, including proton buffering, immune modulation, the detoxification of reactive oxygen and nitrogen species, chelation of metal ions, erythropoiesis, and regulation of the histamine system [10]. It has been used in the treatment of various diseases, such as atopic dermatitis, ageing-related disorders, and metabolic syndrome [11–13]. However, the use of histidine supplementation in sepsis has not been studied and warrants further exploration. In this study, we first investigated T cell differentiation and miR-182 expression in sepsis by establishing a cecum ligation puncture (CLP) model. We then determined the specific role of miR-182 on septic T cells by constructing miR-182 knockout (miR-182$^{-/-}$) mice and performing proteomics and metabolomics. Further, the relationship between histidine metabolism and T cell immune function was investigated through direct regulation of histidine. Finally, the relationship between miR-182, histidine and cellular immune function and prognosis was analyzed in clinical sepsis patients. This revealed the role and molecular mechanism of miR-182 in regulating histidine metabolism to mediate T cell differentiation and immune paralysis in sepsis, which provided a potential intervention target for sepsis immune control.

Materials and Methods

Study Approval

Animal experiments were performed in accordance with protocols approved by the Institutional Animal Care and Use Committee at the First Affiliated Hospital of Wenzhou Medical University (Approval No. 2021-0014) and the National Institutes of Health Guide for the Care and Use of Laboratory Animals. The human study was approved by the Ethics Committee of the First Affiliated Hospital of Wenzhou Medical University (Approval No. 2021-070). Prior to inclusion in the study, all participants were enrolled through written informed consent.

Animal Model of Sepsis and Drug Administration

Male wild-type (WT) and miR-182$^{-/-}$ mice of a C57BL/6J background (age 6–8 weeks) were purchased from GemPharmatech Co. Ltd (Nanjing, China). Mice were housed in a specific pathogen-free (SPF) environment at a temperature of 23–25 °C, with 55 ± 5% humidity and a 12-hour light/dark cycle, with free access to food and water.

The CLP mouse model was established as previously described [14]. In brief, mice were anesthetized by intraperitoneal injection of ketamine (80 mg/kg) and xylazine (5 mg/kg). After disinfection, a 1 cm midline laparotomy was performed in the abdomen. Then the cecum was exposed, and ligated at 1.5 cm position from the tip. Two holes were punctured with an 18-gauge needle, and 1–2 mm feces were extruded before cecum was put back into the abdominal cavity. The abdominal cavity was closed in layers using 5 − 0 silk sutures, followed by fluid resuscitation with 5 mL/100 g saline. Sham animals underwent the same procedure but without cecum ligation and puncture.

At 12 h, 24 h and 48 h after surgery, the animals were euthanized, followed by collection of tissues. The L-histidine treatment groups were administered intraperitoneally with 50 mg/kg, 100 mg/kg, and 200 mg/kg L-histidine immediately after CLP, respectively. In the CLP group, animals received the same volume of normal saline as L-histidine. Survival analysis was observed for up to 96 h.

Isolation of Splenic CD4$^+$ T Cells

Harvested spleens were minced and passed through a 40 μm nylon mesh cell filter. Mononuclear cells were extracted with mouse percoll (TBDscience, Tianjin, China). For CD4$^+$ T cell enrichment, mononuclear cells were incubated with a biotin-conjugated antibody cocktail targeting non-CD4$^+$ cells (10 μl/10^7 cells) at 4 °C for 10 min, followed by antibiotin microbeads (20 μl/10^7 cells) for 15 min. Cells were applied to a negative selection MS column, and the flow-through containing enriched CD4$^+$ T cells was collected. These cells were then stained with PE-anti-CD25 (10 μl/10^7 cells), labeled with anti-PE microbeads, and separated via positive selection: magnetically retained cells yielded CD4$^+$CD25$^+$ Tregs, while the flow-through contained CD4$^+$CD25$^-$ effector T cells (Teff).

Flow Cytometry

After washing with PBS, splenic mononuclear cells were incubated with Fc receptor blocker CD16/32 (clone 2.4G2; BD Pharmingen) and incubated with fluorochrome-conjugated monoclonal antibodies at 4 °C for 30 min in the dark. The antibodies used were as follows: Brilliant Violet 510 CD45 (clone 30-F11; BD Pharmingen), Alexa Fluor 700 CD3 (clone 500A2; BD Pharmingen), Brilliant Violet 786 CD4 (clone GK1.5; BD Pharmingen), PerCP-Cyanine5.5 CD8a (clone 53 − 6.7; BD Pharmingen), APC CD44 (clone IM7; BD Pharmingen), PE/Cyanine7 CD62L (clone MEL-14; BD Pharmingen), BD Horizon Brilliant Blue 515 CD25 (clone PC61; BD Pharmingen), PE IFN-γ(clone XMG1.2; BD Pharmingen), Brilliant Violet 605 IL-4 (clone 11B11;

BD Pharmingen), and Brilliant Violet 650 IL-17 A (clone TC11-18H10; BD Pharmingen). For Tregs staining, cells stained with surface molecules were fixed, permeabilized, and stained intracellularly with Foxp3 using the Transcription Factor Buffer kit (BD Pharmingen) according to the manufacturer's directions. Finally, cells were washed three times, fixed with 0.5% paraformaldehyde, and then analyzed on BD FACS Aria III (BD Biosciences, San Jose, CA, USA).

T-cell Proliferation Assays

To detect proliferation response to experimental sepsis, freshly isolated $CD4^+$ T cells (5×10^4 cells/well), or co-cultured $CD4^+CD25^+$ Tregs (5×10^3cells/well) with $CD4^+CD25^-$ Teff (5×10^4 cells/well) were inoculated into a plate (96-well), and incubated with 5 μg/ml ConA for 68 h. Then MTT (M6494, Invitrogen) was added and incubated for 4 h. The supernatant was removed, and dimethylsulfoxide solution was added to each well to dissolve the formazan. The optical density of the MTT-treated cells was measured using a Spectra MR microplate reader (Dynex, Richfield, MN, USA) at a wavelength of 570 nm.

Quantitative Real Time-PCR

The cellular mRNA was isolated using RNAsimple Total RNA Kit (TIANGEN, Beijing, China). RNA concentration and quality were detected by NanoDrop Lite (Thermo Scientific, ND-LITE). Reverse transcription was performed with RevertAid First Strand cDNA Synthesis Kit (Thermo Scientific, K1622), and the cDNA was subjected to quantitative real-time PCR using PowerTrack SYBR Green Master Mix according to the manufacturer's specification (Thermo Scientific, A46110). Primer sequences were as follows: U6: 5'- CTCGCTTCGGCAGCACA-3' and 5'- AACGCTTCA CGAATTTGCGT-3'; miR-182-5p:5'- GCGCTTTGGCAA TGGTAGAACT-3' and 5'- TGCAGGGTCCGAGGTAT-3'. Data were analyzed using the comparative analysis of relative expression based on ΔΔCT methods.

Western Blotting

Pretreated cells were harvested to lysate with a complex consisting of cold Radioimmunoprecipitation Assay (RIPA) lysis, protease inhibitors and phosphatase inhibitors. After incubation on ice for 30 min, the lysates were centrifuged with 12,000 rpm at 4 °C for 25 min. The supernatants were quantified using a BCA protein Assay Kit (Thermo Scientific, 23227) and then boiled at 100 °C for 10 min after mixing with SDS-loading buffer. Proteins were separated by SDS-PAGE and transferred to a polyvinylidene fluoride membrane (Millipore, IPVH00010), then blocked with 5% milk in TBST at room temperature for 1.5 h. The membranes were incubated with the indicated primary antibodies overnight at 4 °C. The following primary antibodies were used: anti-HAL antibody (Abcam, ab154063, 1:1000), anti-HDC antibody (Abcam, ab137571, 1:1000), anti-ALDH1A1 antibody (Abcam, ab52492, 1;1000), anti-FOXO3 antibody (Abcam, ab23683, 1:1000). Then, the membranes were washed with TBST and incubated with a secondary antibody for 1 h at room temperature. Immunoreactive bands were visualized by an Invitrogen iBright CL 1500 system and densitometrically analyzed using Image J software.

Histological Analysis

Lung tissues and kidneys samples were collected, fixed in 4% paraformaldehyde, embedded in paraffin and then 5 μm slices were made. Hematoxylin and eosin (H&E) staining was routinely performed. The slices were observed under an optical microscope (NIKON Eclipse Ci, Japan).

Measurement of Histidine and Cytokine Levels

The levels of histidine, IL-10, and TNF-β in plasma and supernatants were measured by ELISA kits according to the manufacturers' protocols. All the data were analyzed using a Spectra MR microplate reader (Dynex, Richfield, MN, USA).

Metabolomics

The $CD4^+$ T cells from the WT group and the miR-182 group post CLP were collected and stored at −80°C for metabolomics procedure. Metabolomics analysis was executed by Biotree Technology (Shanghai, China). Briefly, metabolites were extracted by scraping the cells after adding 4 °C methanol and lysing with a cell pulverizer. Liquid chromatography/mass spectrometry (LC/MS) data were analyzed by Compound Discoverer 2.1 software (Thermo Fisher, USA). Identified metabolites or intensity matrices of identified and annotated metabolites were processed using Metaboanalyst 5.0 for clustering heat maps and principal component analysis.

Proteomics

Proteomic analysis was conducted by Biotree Technology (Shanghai, China). Briefly, cellular proteins were extracted via centrifugation and lysis. Samples were then digested, labeled, separated and protein expression was analyzed by liquid chromatography-tandem mass spectrometry (LC-MS/MS). Then protein annotation, functional classification,

functional enrichment and cluster analysis were performed for bioinformatics analysis.

Human Patients and Sample Collection

Clinical data and plasma samples used in this study were obtained from 128 patients treated for sepsis between June 2020 and May 2021 in the emergency intensive care unit of the First Affiliated Hospital of Wenzhou Medical University. Inclusion criteria were as follows: (1) over 18 years old, and the gender is not limited; (2) meet Sepsis-3 criteria for sepsis or septic shock; and (3) provided written informed consent. The exclusion criteria were as follows: (1) women who are pregnant or breastfeeding; (2) those who are expected to survive less than 48 h and have incomplete clinical information; and (3) those who had an infection requiring antibiotic treatment in the last month, were hospitalized for an infection, or had chemotherapy or radiation therapy within the last year. The clinical data and plasma were also collected from 50 healthy volunteers who underwent health checkups at the Physical Examination Center of the First Affiliated Hospital of Wenzhou Medical University during the same period.

Statistics

Data were expressed as the mean ± SEM, and statistical analysis was performed using GraphPad Prism 9 (GraphPad Software). Three independent experiments were performed at least. Unpaired two-tailed t-tests (for two groups) or one-way ANOVA by Tukey's test (for three or more groups) were performed on data. Kaplan-Meier curves were used to compare the time-to event survival. $P < 0.05$ was considered statistically significant.

Results

T Cells Show Impaired Differentiation and Immunosuppression in Septic Mice

To understand the impact of sepsis on T cell differentiation and immune function, we constructed a CLP model to induce experimental sepsis. Splenic single-cell suspensions were obtained to evaluate the expression of T cell phenotype markers at different time points. Cells were clustered and visualized based on the expression of their surface markers using Uniform Manifold Approximation and Projection (UMAP) for dimensionality reduction [15]. Splenocytes were identified following UMAP-based dimensionality reduction (Fig. 1A). The surface markers of T cells (CD45, CD3, CD4, and CD8) were highly enriched and distinctly clustered. Meanwhile, IFN-γ, IL-4, CD25, Foxp3, and CD44 had lower expression levels, whereas IL-17 and CD62L had the lowest expression levels.

Fig. 1 Impaired differentiation and immunosuppression of T cells in septic mice. (**A**) UMAP plots showing the expression of various markers in splenic lymphocytes from sham-operated mice and septic mice at 12 h, 24 h and 48 h after CLP. (B) UMAP plots illustrating the dynamic changes in splenic lymphocyte populations in mice treated as described in (**A**). (**C**) Representative flow cytometry plots and statistical analysis of the proportions of $CD3^+$ T cells, $CD4^+/CD3^+$ T cells, and $CD8^+/CD3^+$ T cells in mice treated as described in (**A**). (**D**) Representative flow cytometry plots and statistical analysis of the proportions of Th1 ($CD4^+IFN\text{-}\gamma^+$), Th2 ($CD4^+IL\text{-}4^+$) cells, Th17 ($CD4^+IL\text{-}17^+$) cells, and Tregs ($CD4^+CD25^+Foxp3^+$) in mice treated as described in (**A**). (**E**) Representative flow cytometry plots and statistical analysis of the proportions of $CD4^+$ TEM, $CD4^+$ TEMRA, $CD8^+$ TEM, and $CD8^+$ TEMRA cells in mice treated as described in (**A**). (**F**) Quantification of $CD3^+$ T cell counts in the spleens of mice treated as described in (**A**). (**G**) $CD4^+$ T cell proliferation ability assessed using the MTT assay in mice treated as described in (**A**). Data were shown as mean ± SEM. ns, non-significance; $*p < 0.05$; $**p < 0.01$; $***p < 0.001$

The proportion of different cell types in each group was shown in Fig. 1B, which showed that $CD3^+$ T cells, $CD4^+$ T cells, and $CD8^+$ T cells were significantly reduced in septic mice. T cells were primarily categorized into $CD3^+CD4^+$ T cells and $CD3^+CD8^+$ T cells (the gating strategy was provided in Supplementary Fig. S1). As shown in Fig. 1C, the number of $CD3^+$ T cells was significantly reduced in the CLP mice, which was consistent with other studies [16–19]. Meanwhile, we sorted out $CD4^+$ T cells and $CD8^+$ T cells from $CD3^+$ T cells. Flow cytometry analysis showed that within the remaining $CD3^+$ T-cell population, the proportion of $CD4^+$ T cells increased, whereas $CD8^+$ T cells decreased at 24 h post-CLP. Following activation, $CD4^+$ T cells underwent differentiation into specialized subsets: Th1, Th2, Th17, and Tregs. Intriguingly, flow cytometry analysis revealed that the relative proportions of both Th1 and Th2 cells within the $CD4^+$ T-cell population were significantly elevated in CLP mice compared to sham-operated animals (Fig. 1D), suggesting a dysregulated immune response during sepsis. No significant change was observed in the proportion of Th17 cells in the spleens of septic mice, while the proportion of Tregs was significantly increased. Then cells were classified into initial cells, central memory T cells, effector memory T cells (TEM) and terminally Differentiated Effector Memory T cells (TEMRA) by staining CD62L and CD44. Since CD62L was found to be largely unexpressed, we quantified the expression of $CD4^+$ TEM, $CD4^+$ TEMRA, $CD8^+$ TEM, and $CD8^+$ TEMRA cell populations. The proportion of $CD4^+$ TEM was increased and $CD4^+$ TEMRA was decreased after CLP, whereas the changes in the proportions of $CD8^+$ TEM and $CD8^+$ TEMRA were not significant (Fig. 1E). To further evaluate the immune function of T cells, we quantified the number of splenic $CD3^+$T cells, as shown in Fig. 1F. Compared with the Sham

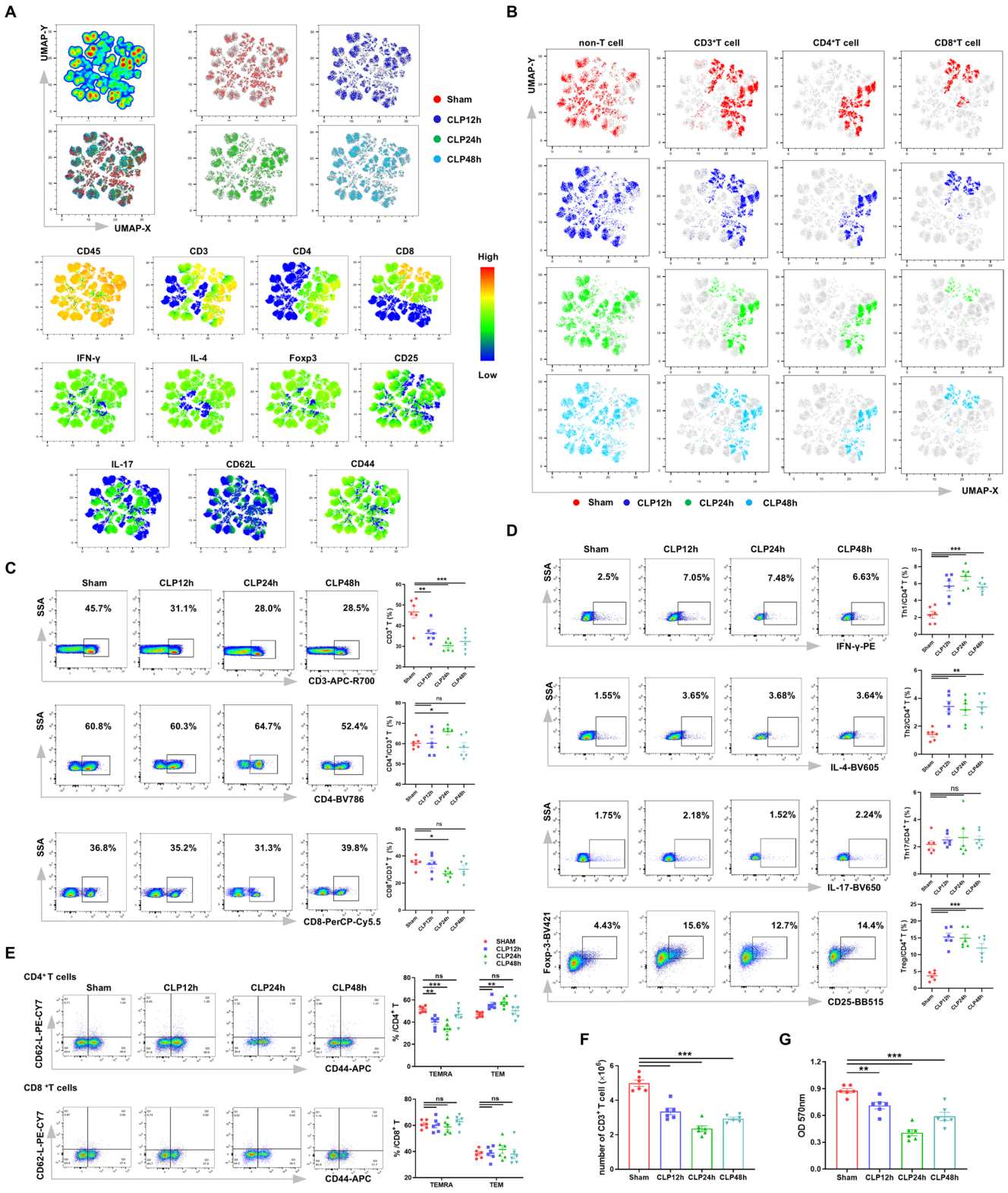

group, the number of $CD3^+$T cells in the CLP group was decreased, with the most pronounced decline observed at 24 h. The proliferation ability was a major indicator of T cell immune function. MTT was used to assess the proliferation ability of $CD4^+$ T cells in vivo (Fig. 1G). Compared with the Sham group, the proliferation ability of the CLP group was decreased, and found to be most pronounced at 24 h.

Collectively, these findings indicate impaired T-cell differentiation and immunosuppression in septic mice.

miR-182 Impairs T Cell Immune Function and Differentiation in Septic Mice

To investigate the role of miR-182 in sepsis, we assessed its expression levels in peripheral blood and splenic lymphocytes at 12 h, 24 h and 48 h after CLP induction. Our qPCR analysis revealed a significant upregulation of miR-182 in both peripheral blood and splenic lymphocytes in CLP-induced septic mice, with the highest expression detected at 24 h post-CLP (Fig. 2A, B). To further investigate whether elevated miR-182 contributed to the immunosuppression of $CD4^+$ T cells, we evaluated the T cell subtypes, proliferative capacity, and cytokine expression in T cells isolated from WT mice and miR-182-/- mice after CLP treatment. The UMAP plots revealed increased populations of $CD3^+$, $CD4^+$, and $CD8^+$ T cells in the splenic lymphocytes of miR-$182^{-/-}$ mice after CLP, compared to WT mice (Fig. 2C, D). Furthermore, flow cytometry analysis showed an increased in $CD3^+$ T cells in the splenic lymphocytes of miR-$182^{-/-}$ mice after CLP (Fig. 2E). Compared to the WT-CLP group, the proportion of $CD4^+$ T cells was increased, while that of $CD8^+$ T cells was decreased in the miR-$182^{-/-}$-CLP group. Moreover, knockout of miR-182 resulted in reduced proportions of Th1 cells, Th2 cells, Th17 cells, and Tregs following CLP treatment (Fig. 2F). We also evaluated the proportions of $CD4^+$ TEMRA, $CD4^+$ TEM, $CD8^+$ TEMRA, and $CD8^+$ TEM cells. As shown in Fig. 2G, there was no significant difference in the proportions of $CD4^+$ TEMRA and $CD4^+$ TEM cells between the miR-$182^{-/-}$-CLP group and the WT-CLP group. However, the proportion of $CD8^+$ TEMRA cells was increased while that of $CD8^+$ TEM cells was decreased in miR-$182^{-/-}$ mice compared to the WT mice after CLP. The shift from $CD8^+$ TEM to TEMRA subsets in miR-$182^{-/-}$ mice may reflect altered differentiation or survival of cytotoxic T lymphocytes, warranting further investigation. To further explore the impact of miR-182 knockout on T cell immune function, we measured the number of splenic $CD3^+$ T cells. As shown in Fig. 2H, the number of $CD3^+$ T cells was notably higher in the miR-$182^{-/-}$ -CLP group compared to the WT-CLP group. Additionally, T cell proliferation was assessed using the MTT assay. The results showed that miR-182 knockout enhanced T cell proliferation post CLP (Fig. 2I). Splenic Tregs were significantly reduced after knockout of miR-182 in septic mice. Therefore, we further investigated the effect of miR-182 on Tregs. Using flow cytometric sorting, we isolated $CD4^+CD25^+$ Tregs and $CD4^+CD25^-$ Teff, with a purity of over 90% (Fig. 2J). Compared with the WT-CLP group, the ability of miR-$182^{-/-}$ $CD4^+CD25^+$ T cells to secrete IL-10 and TGF-β was significantly reduced (Fig. 2K, L). For proliferation assays, $CD4^+CD25^+$ Tregs and $CD4^+CD25^-$ effector T cells were co-cultured at a 1:10 ratio under ConA stimulation (5 μg/mL). Because $CD4^+CD25^-$ effector T cells are highly responsive to ConA-induced proliferation, while Tregs exhibit limited proliferative capacity under these conditions [20], the observed proliferation predominantly reflects the activity of $CD4^+CD25^-$ effector T cells. As shown in Fig. 2M, knockout of miR-182 reduced the immunosuppressive capacity of $CD4^+CD25^+$ Tregs, leading to enhanced proliferation of $CD4^+CD25^-$ Teff. Collectively, these results suggest that miR-182 mediated the immunosuppression of $CD4^+$ T cells, especially Tregs, in septic mice.

Fig. 2 miR-182 impairs T cell immune function and differentiation in septic mice. (**A**) The mRNA expression levels of miR-182 in peripheral blood from sham-operated mice and septic mice at 12 h, 24 h and 48 h after CLP. **(B)** The mRNA expression levels of miR-182 in splenic lymphocytes from mice treated as described in (**A**). (**C**) UMAP plots showing the expression of various markers in splenic lymphocytes from miR-$182^{-/-}$ mice and WT mice at 24 h after CLP. **(D)** UMAP plots showing changes in splenic lymphocyte populations in mice treated as described in (**C**). (**E**) Representative flow cytometry plots and statistical analysis of the proportions of $CD3^+$ T cells, $CD4^+/CD3^+$ T cells, and $CD8^+/CD3^+$ T cells in splenic lymphocytes from mice treated as described in (**C**). (**F**) Representative flow cytometry plots and statistical analysis of the proportions of Th1 ($CD4^+IFN\text{-}\gamma^+$) cells, Th2 ($CD4^+IL\text{-}4^+$) cells, Th17 ($CD4^+IL\text{-}17^+$) cells, and Tregs ($CD4^+CD25^+Foxp3^+$) in splenic lymphocytes from mice treated as described in (**C**). (**G**) Representative flow cytometry plots and statistical analysis of the proportions of $CD4^+$ TEM, $CD4^+$ TEMRA, $CD8^+$ TEM, and $CD8^+$ TEMRA cells in splenic lymphocytes from mice treated as described in (C). **(H)** Total number of $CD3^+$ T cells in the spleens of mice treated as described in (C). **(I)** $CD4^+$ T cell proliferation assessed using the MTT assay in mice treated as described in (**C**). (**J**) Representative flow cytometry plots showing the gating strategy used to distinguish $CD4^+CD25^+$ Tregs and $CD4^+CD25^-$ Teff. **(K, L)** Supernatant levels of IL-10 and TGF-β in cultured $CD4^+CD25^+$ Tregs from mice treated as described in (**C**). **(M)** $CD4^+CD25^+$ Tregs from mice treated as described in (**C**) were co-cultured with $CD4^+CD25^-$ Teff at a ratio of 1:10 for 68 h, and the proliferation of cells within the co-culture system (primarily reflecting Teff proliferation) was assessed using the MTT assay. Data were shown as mean ± SEM. ns, non-significance; $^*p<0.05$; $^{**}p<0.01$; $^{***}p<0.001$

Knockout of miR-182 Protects Septic Mice

To further investigate the effect of miR-182 knockout on organ pathology in septic mice, we collected lung and kidney tissues 24 h post-CLP. Histopathological changes were assessed using H&E staining. As shown in Fig. 3A, WT mice exhibited alveolar edema, hemorrhage, and inflammatory cell infiltration in the lungs 24 h post-CLP, whereas miR-$182^{-/-}$ mice showed less severe lung injury. Similarly, Fig. 3B showed that, compared to the WT-CLP group, miR-$182^{-/-}$ mice displayed less severe kidney pathology 24 h post-CLP, with less disruption of the renal tubular structure, reduced glomerular swelling, and fewer infiltrating

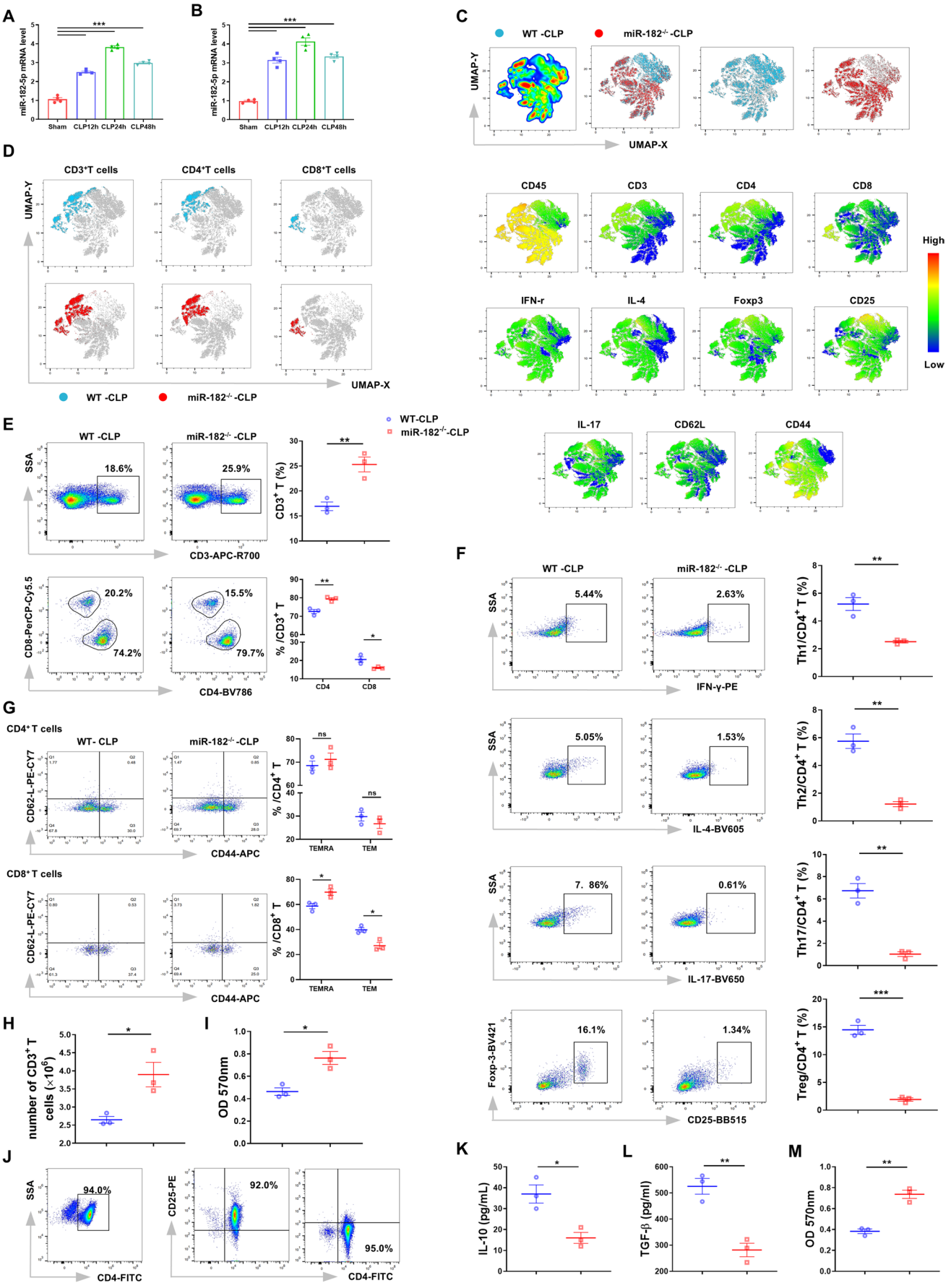
A
B
miR-182-5p mRNA level
Sham
CLP12h
CLP24h
CLP48h
C
WT -CLP
miR-182-/- -CLP
UMAP-Y
UMAP-X
CD45
CD3
CD4
CD8
IFN-r
IL-4
Foxp3
CD25
IL-17
CD62L
CD44
High
Low
D
CD3+T cells
CD4+T cells
CD8+T cells
E
WT-CLP
miR-182-/-CLP
SSA
18.6%
25.9%
CD3-APC-R700
CD3+ T (%)
CD8-PerCP-Cy5.5
20.2%
74.2%
15.5%
79.7%
CD4-BV786
% /CD3+ T
F
5.44%
2.63%
IFN-γ-PE
Th1/CD4+ T (%)
5.05%
1.53%
IL-4-BV605
Th2/CD4+ T (%)
7. 86%
0.61%
IL-17-BV650
Th17/CD4+ T (%)
16.1%
1.34%
Foxp-3-BV421
CD25-BB515
Treg/CD4+ T (%)
G
CD4+ T cells
WT- CLP
CD62-L-PE-CY7
CD44-APC
% /CD4+ T
TEMRA
TEM
CD8+ T cells
% /CD8+ T
H
number of CD3+ T cells (×10^6)
I
OD 570nm
J
94.0%
92.0%
95.0%
CD4-FITC
CD25-PE
K
IL-10 (pg/mL)
L
TGF-β (pg/ml)
M
OD 570nm

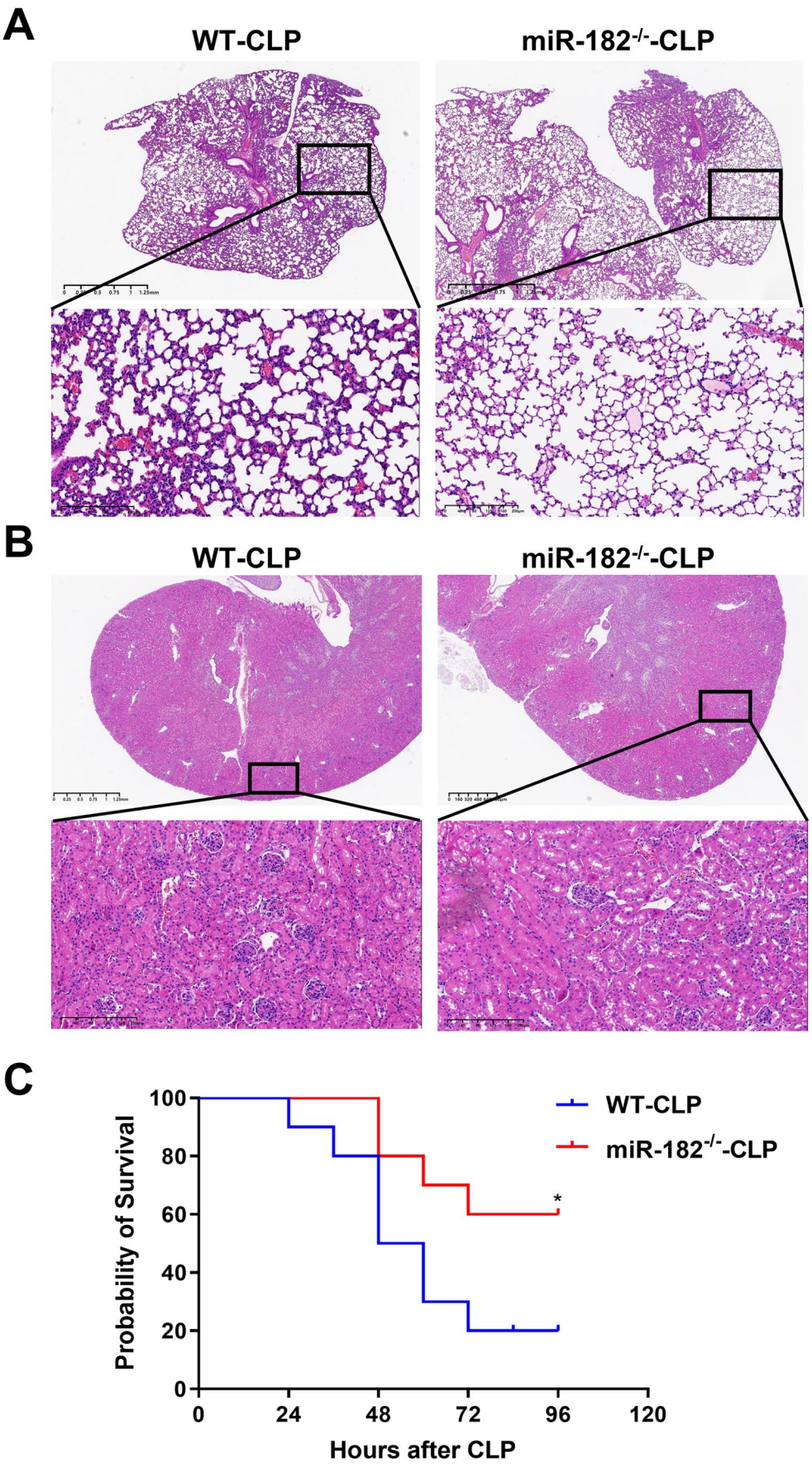

Fig. 3 Knockout of miR-182 protects septic mice. (**A**) H&E staining of lung tissues from miR-182$^{-/-}$ mice and WT mice 24 h post-CLP. (**B**) H&E staining of renal tissues from mice treated as described in (**A**). (**C**) Survival rates of mice treated as described in (**A**) over 96 h post-CLP. Data were shown as mean ± SEM. ns, non-significance; $^{*}p < 0.05$; $^{**}p < 0.01$; $^{***}p < 0.001$

inflammatory cells. Furthermore, survival rates were evaluated in both groups post-CLP (Fig. 3C), and the miR-182$^{-/-}$-CLP group had a significantly higher survival rate than the WT-CLP group, suggesting better resistance to septic shock. These findings support the idea that miR-182 deficiency mitigates sepsis-induced organ damage and improves survival in mice.

Integrated Metabolomic and Proteomic Profiling of CD4$^+$ T Cells in miR-182 Knockout Septic Mice

To explore the potential mechanism by which miR-182 regulates T cells, we employed a combined metabolomic and proteomic analysis of purified CD4$^+$ T cells. Orthogonal partial least squares discriminant analysis (OPLS-DA) of metabolomic data revealed a distinct separation between WT and miR-182$^{-/-}$ groups (Fig. 4A). A total of 465 metabolites were detected in positive-ion mode. Using $P<0.05$ and variable importance in projection (VIP)>1 as the significance criteria, 31 metabolites were identified as significantly different between the two groups (Fig. 4B, C). Notably, the level of 1-methylhistamine was significantly lower in the miR-182$^{-/-}$ group compared to the WT group ($p=0.0124$, Fig. 4D). Pathway analysis of the differentially expressed metabolites (DEMs) identified histidine metabolism, tryptophan metabolism, and aminoacyl-tRNA biosynthesis as the most enriched pathways (Fig. 4E). To gain a comprehensive understanding of the effect of miR-182 on CD4$^+$ T cells, we further performed proteomic analyses. A total of 2044 proteins were detected, among which 49 were significantly upregulated and 58 were downregulated in the miR-182$^{-/-}$ group ($p<0.05$, fold-change<0.83 or >1.2) (Fig. 4F, G). Interestingly, histidine ammonia-lyase (HAL) and acetaldehyde dehydrogenase-1 (ALDH1A1) were significantly reduced in the miR-182$^{-/-}$ group compared to the WT group (Fig. 4H, I). To explore the relationship between metabolites and proteins, we performed a multi-omics analysis integrating proteomic and untargeted metabolomics data. We found that the two differentially expressed proteins, HAL and ALDH1A1, along with the differentially expressed metabolite 1-methylhistamine, were closely associated with histidine metabolism (Fig. 4J). KEGG pathway analysis further revealed that the knockout of miR-182 impaired histidine catabolism, suggesting histidine accumulation in miR-182$^{-/-}$ mice (Fig. 4K-M). Finally, we validated these findings via Western blot and ELISA. The expression levels of histidine decarboxylase (HDC), HAL, and ALDH1A1 were lower in the miR-182$^{-/-}$ group compared to the WT group (Fig. 4N-Q), whereas histidine levels in the cell supernatant were elevated (Fig. 4R). In summary, these data demonstrate that miR-182 modulates CD4$^+$ T cell function through histidine metabolism.

Histidine Supplementation Enhances T Cell Immune Function in Septic Mice

Based on the previous results, we investigated the effect of histidine supplementation on T cells in septic mice. We administered L-histidine immediately after CLP via intraperitoneal injection at doses of 50 mg/kg, 100 mg/kg, and 200 mg/kg. Flow cytometry analysis revealed that, compared to the CLP group, the proportion of CD3$^+$ T cells was increased significantly in the CLP+L-histidine groups (Fig. 5A). Among CD3$^+$ T cells, the proportion of CD4$^+$ T cells decreased, while that of CD8$^+$ T cells increased in the CLP+L-histidine groups compared to the CLP group. Furthermore, the proportions of Th1 cells, Th2 cells, and Tregs significantly decreased in the CLP+L-histidine groups, while the proportion of Th17 cells did not change significantly compared to the CLP group (Fig. 5B).

The marked reduction in Treg proportions and cytokine secretion (Fig. 5B-D) suggested that L-histidine preferentially modulated Treg-mediated immunosuppression. Additionally, MTT assays showed that CD4$^+$CD25$^-$ Teff, co-cultured with CD4$^+$CD25$^+$ Tregs, exhibited enhanced proliferative capacity when L-histidine was added (Fig. 5E).

To predict the potential target genes of miR-182, we screened for miR-182 targets using 10 different databases (miRWalk, Microt4, miRanda, miRDB, miRMap, miRNAMap, PITA, RNA22, RNAhybrid, and TargetScan). A total of 26 common target genes were identified, including Adcy6, Prdm1, Bmi1, Clock, Fbn1, Gnaq, Ppp1r13b, Gria3, Foxo3, Fam134b, Smc6, Zfand4, Dusp6, Paip2, Nrn1, Dcaf12, Taf15, Wdr44, Wasl, Pabpc5, Ube3c, Pdzd8, Etl4, Zbtb41, Slitrk4, and Frs2 (Fig. 5F). Among these, Foxo3 regulates immune homeostasis and tolerance by controlling immune cell development and function [21–23]. It is closely linked to T cell differentiation and is a likely target gene of miR-182. To validate this hypothesis, we assessed FOXO3 protein expression in the WT group and the miR-182$^{-/-}$ group. The results showed that FOXO3 was significantly downregulated following miR-182 knockout, confirming that miR-182 regulates T cell immune function through FOXO3 (Fig. 5G). These results indicated that L-histidine supplementation improved T cell immune function, especially by regulating the function of Tregs. In addition, these findings suggest that miR-182 may regulate histidine metabolism to affect T-cell immune function and differentiation through the modulation of its target gene, Foxo3.

miR-182 as a Potential Predictor for sepsis Severity and Prognosis

To evaluate the prognostic value of plasma miR-182 in sepsis, we enrolled 128 sepsis patients (46 with sepsis and 82

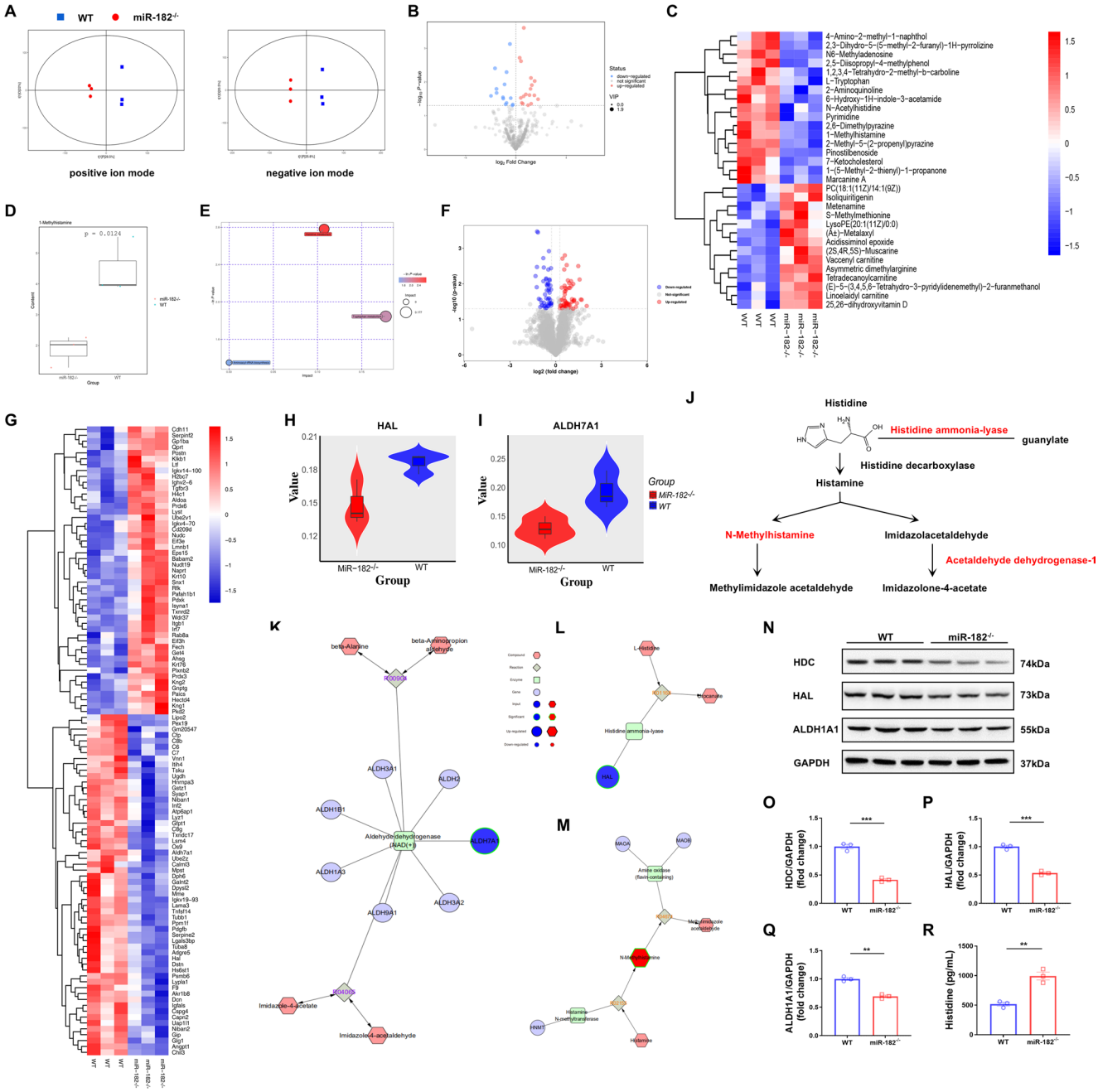

Fig. 4 Metabolomic and proteomic profiling of CD4$^+$ T cells following miR-182 knockout in septic mice. (**A**) OPLS-DA score plots of CD4$^+$ T cells from miR-182$^{-/-}$ and WT mice in positive-ion mode (left) and negative-ion mode (right). (**B**) Volcano plot based on DEMs in CD4$^+$ T cells from mice described in (**A**). (**C**) Heatmap displaying the relative abundance of 31 key metabolites identified in CD4$^+$ T cells from mice described in (A). **(D)**Relative levels of 1-Methylhistamine in CD4$^+$ T cells from mice described in (**A**). (**E**) Pathway analysis of key metabolites in CD4$^+$ T cells from mice described in **(A)**. **(F)** Volcano plot showing differentially expressed proteins in CD4$^+$ T cells from mice described in (**A**). (**G**) Heatmap displaying the relative abundance of 107 key proteins identified in CD4$^+$ T cells from mice described in (**A**). (**H**, **I**) Violin plots showing the expression levels of HAL and ALDH1A1 in CD4$^+$ T cells from mice described in (**A**). (**J**) Schematic representation of the histidine metabolism pathway, highlighting key enzymes and metabolic intermediates. (**K**, **L**, **M**) KEGG pathway analysis of histidine metabolism and related metabolites, highlighting key enzymes and their regulation. (**N**, **O**, **P**, **Q**) Western blot analysis of HDC, HAL, and ALDH1A1 expression at 24 h post-CLP in CD4$^+$ T cells from mice described in (**A**). (**R**) ELISA analysis showing histidine levels in the supernatants of CD4$^+$ T cells from mice described in (**A**). Data were shown as mean ± SEM. ns, non-significance; $^*p<0.05$; $^{**}p<0.01$; $^{***}p<0.001$

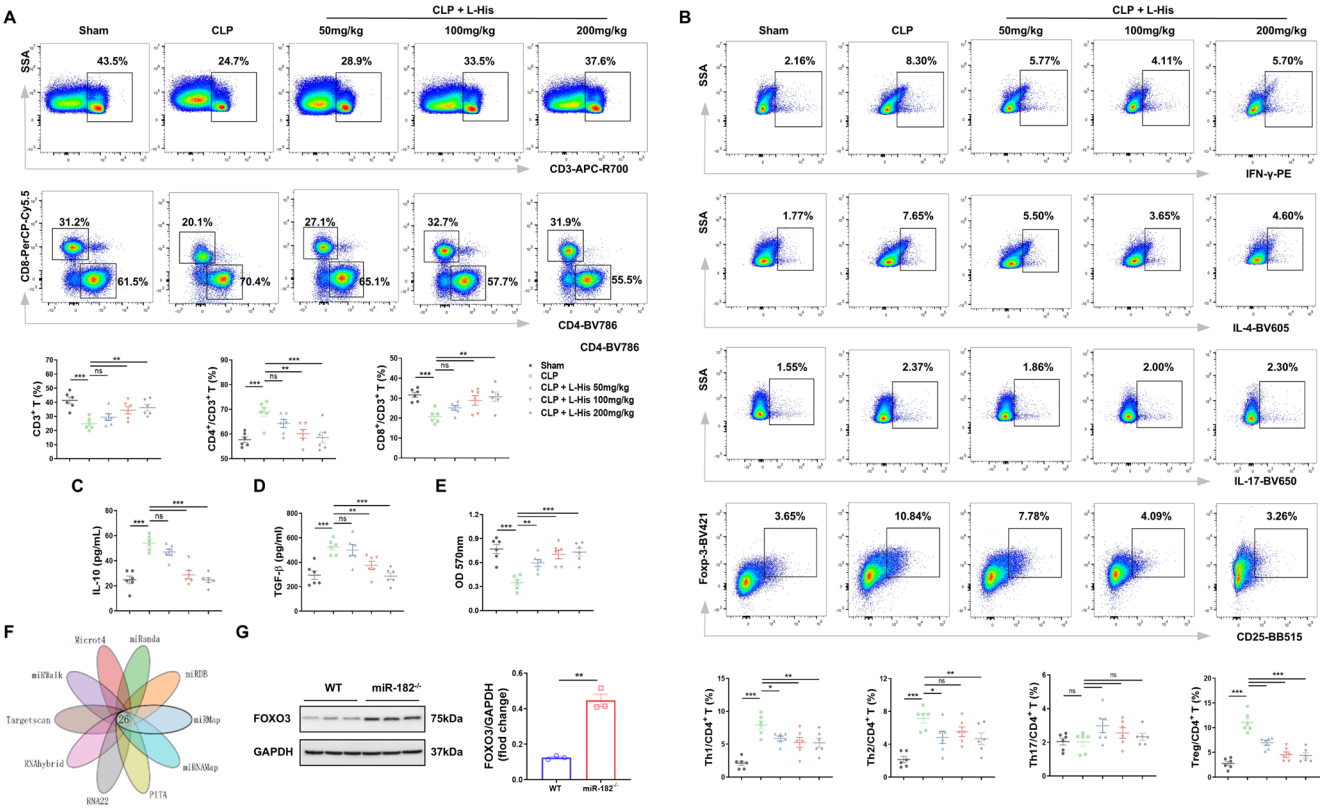

Fig. 5 L-histidine supplementation improves T cell immune function in septic mice. (**A**) Representative flow cytometric analysis and statistical analysis of the proportions of $CD3^+$ T cells, $CD4^+/CD3^+$ T cells, and $CD8^+/CD3^+$ T cells in mice treated with sham operation, CLP, CLP + 50 mg/kg L-histidine (i.p.), CLP + 100 mg/kg L-histidine (i.p.), and CLP + 150 mg/kg L-histidine (i.p.). (**B**) Representative flow cytometric analysis and statistical analysis of the proportions of Th1 ($CD4^+IFN\text{-}\gamma^+$) cells, Th2 ($CD4^+IL\text{-}4^+$) cells, Th17 ($CD4^+IL\text{-}17^+$) cells, and Tregs ($CD4^+CD25^+Foxp3^+$) in mice treated as described in (**A**). (**C**, **D**) Supernatant levels of IL-10 and TGF-β in cultured $CD4^+CD25^+$ T cells from mice treated as described in (A). **(E)** $CD4^+CD25^+$ Tregs from mice treated as described in (**A**) were co-cultured with $CD4^+CD25^-$ Teff at a ratio of 1:10 for 68 h. MTT assay was used to assess the proliferation of cells within the co-culture system (primarily reflecting Teff proliferation). (**F**) Venn diagram showing the 26 common target genes of miR-182 identified by ten databases. (**G**) Western blotting analysis of FOXO3 expression in the WT group and the miR-$182^{-/-}$ group. Data were shown as mean ± SEM. ns, non-significance; $^*p<0.05$; $^{**}p<0.01$; $^{***}p<0.001$

with septic shock) and 50 age- and sex-matched healthy controls. The baseline characteristics were summarized in Table 1. The primary infection sources were hepatobiliary (21.09%), urinary tract (14.06%), gastrointestinal (13.28%), pulmonary (11.72%), and others (15.63%). Patients with septic shock exhibited significantly higher APACHE II scores (16 (11–21) vs. 14 (10–17), $p=0.0044$), SOFA scores (5 (3–9) vs. 9 (6-11.75), $p<0.0001$), lactate levels (3.398 ± 0.36 vs. 6.11 ± 0.74 mmol/L, $p=0.0014$), and procalcitonin (PCT) levels (28.65 ± 5.59 vs. 62.87 ± 6.831 mg/L, $p<0.0001$) compared to sepsis patients. Although 28-day mortality was higher in septic shock (17.39% vs. 24.35%), the difference was not statistically significant ($p=0.44$). Plasma miR-182 levels were markedly elevated in sepsis patients versus controls (Fig. 6A), with further increases in septic shock (Fig. 6B). Moreover, plasma miR-182 levels in sepsis patients were not significantly associated with the number of organ failures (Fig. 6C). As shown in Fig. 6D, E, miR-182 concentrations positively correlated with APACHE II ($r=0.2068$, $p=0.0192$) and SOFA scores ($r=0.1747$, $p=0.0485$). Histidine levels were reduced in sepsis patients compared to controls (Fig. 6F) and further decreased in non-survivors versus survivors (Fig. 6G). Correlation analysis showed that histidine levels were negatively correlated with plasma miR-182 concentrations ($r=0.2118$, $p=0.01164$) (Fig. 6H). Receiver operating characteristic (ROC) analysis revealed that miR-182 (AUC = 0.735) and histidine (AUC = 0.676) had comparable predictive accuracy for 28-day mortality to APACHE II (AUC = 0.702) and SOFA (AUC = 0.695), with no significant differences in AUC values (Fig. 6I; Table 2). Optimal cutoffs were 31.9 ng/mL for miR-182 (81.5% sensitivity, 71.3% specificity) and 10 ng/mL for histidine (74.1% sensitivity, 64.4% specificity). Kaplan-Meier analysis confirmed that patients with miR-182 < 31.9 ng/mL or histidine ≥ 10 ng/mL had significantly improved survival (log-rank $p<0.001$) (Fig. 6J, K).

Table 1 Baseline characteristics of the study population

	Healthy controls	Sepsis	Septic shock	*p* value
Numbers	50	46	82	-
Age, years	61 (52–73)	67 (55.75-75)	65 (54–73)	0.97
Male, n (%)	22 (44%)	22 (48%)	43 (52%)	0.587
Site of infection, n (%)				
Lung	-	7 (15.22)	8 (9.76%)	
Skin and soft tissue	-	4 (8.69%)	7 (8.54)	
Urinary tract	-	4 (8.69%)	14 (17.07%)	
Gastrointestinal	-	5 (10.87%)	12 (14.63%)	
Abdominal	-	5 (10.87%)	5 (6.10%)	
Hepatobiliary	-	9 (19.56%)	18 (21.95%)	
Blood	-	5 (10.87%)	5 (6.10%)	
Others	-	7 (15.22)	12 (15.85%)	
Laboratory value, mean ± SEM				
PCT, mg/L	-	28.65 ± 5.59	62.87 ± 6.83	< 0.0001
CRP, mg/L	-	117.4 ± 11.16	136.9 ± 9.42	0.086
Lactate, mmol/L	-	3.398 ± 0.36	6.11 ± 0.74	0.0014
APACHE II score	-	16 (11–21)	14 (10–17)	0.0044
SOFA score	-	5 (3–9)	9 (6-11.75)	< 0.0001
28-day mortality, n (%)	-	8 (17.39%)	19 (24.35%)	0.44

PCT Procalcitonin, *CRP* C-reactive protein, *APACHE II* acute physiology and chronic health evaluation score, *SOFA* sequential organ failure assessment score

Notably, our results show that plasma miR-182 is associated with the severity of sepsis and serves as a promising prognostic biomarker for 28-day mortality.

Discussion

In this study, we demonstrated that the significant upregulation of miR-182 in septic mice contributed to abnormal T cell differentiation and impaired immune function. Furthermore, we revealed that miR-182 regulated histidine metabolism, and histidine supplementation improved T cell immune dysfunction in sepsis. Mechanistically, miR-182 knockout reduced FOXO3 expression, which may indirectly reduce histidine catabolic enzymes (HAL/ALDH1A1) through transcriptional regulation. These findings enhanced our understanding of the immune mechanisms involved in sepsis.

T cells, particularly $CD4^+$ subsets, play a critical role in sepsis-induced immune dysfunction [24]. Decreased lymphocyte numbers are a hallmark of lymphocyte functional depletion [25]. The quantity of $CD4^+$ and $CD8^+$ T cells and their subtypes are important indicators to assess the immune status in sepsis. Our findings showed a significant reduction in $CD4^+$ and $CD8^+$ T cells after CLP, consistent with previous studies [26–28]. While Th1 and Th2 proportions increased in our CLP model (likely reflecting early immune hyperactivation), Th17 levels remained unchanged, contrasting with reports linking Th17 expansion to late-stage sepsis severity [29, 30]. This discrepancy may stem from differences in experimental timing or pathogen-specific immune responses. Changes of Th17 cells in sepsis remain to be confirmed by further studies. Tregs enhance Fas/Fas Ligand (FasL)-mediated monocyte apoptosis and neutrophil apoptosis following endotoxin stimulation [31, 32]. The increase in Tregs during sepsis is positively correlated with T-cell anergy, a hyporesponsive state to antigen stimulation [33]. We observed a significant increase in the proportion of Tregs, consistent with previous studies [34–37]. Therefore, further investigation is needed to elucidate the regulatory role of Tregs in the immune response during sepsis. TEM cells do not express CD62L, a molecule involved in homing to lymph nodes. Instead, they circulate continuously in peripheral tissues, blood, and the spleen, migrating to peripheral inflammatory tissues to exert rapid effector functions with low proliferative capacity and mediate protective memory [38, 39]. Our study showed that during the acute phase of sepsis, $CD4^+$ T cells in the spleen underwent differentiation from TEMRA to TEM, mediating rapid effector functions. In contrast, no significant abnormalities were observed in the differentiation of $CD8^+$ memory T cells. As this study only observed memory T cell changes within 48 h, further experiments are needed for validation.

miRNAs are important regulators of the T cell immune response [40]. The loss of nearly all miRNAs during early T cell development leads to increased thymocyte apoptosis and a reduction in thymocyte numbers [41, 42]. Knockout of Dicer in later developmental stages further underscores

Fig. 6 miR-182 may be used as a predictor to assess severity and prognosis of septic patients. (**A**) Plasma miR-182 concentrations in healthy controls and sepsis patients. (**B**) Plasma miR-182 concentrations in healthy controls, septic patients, and septic shock patients. (**C**) Plasma miR-182 concentrations in septic patients with more than 2 organ failures and with 2 or fewer organ failures. (**D**) The correlation between plasma miR-182 concentrations and APACHE II scores. (**E**) The correlation between plasma miR-182 concentrations and SOFA scores. (**F**) Plasma histidine concentrations in healthy controls and sepsis patients. (**G**) Plasma miR-182 concentrations in the sepsis survivor group and the sepsis non-survivor group. (**H**) The correlation between plasma miR-182 concentrations and histidine concentrations. (**I**) ROC curve analyses of miR-182, histidine, lactate, APACHE II scores, and SOFA scores for predicting 28-day mortality in septic patients. (**J**) Kaplan-Meier curves of 28-day mortality in patients with sepsis, stratified by the optimal cut-off value of miR-182 concentrations. (**K**) Kaplan-Meier curve of 28-day mortality in patients with sepsis, stratified by the optimal cut-off value of histidine concentrations. Data were shown as mean ± SEM. ns, non-significance; $^*p < 0.05$; $^{**}p < 0.01$; $^{***}p < 0.001$

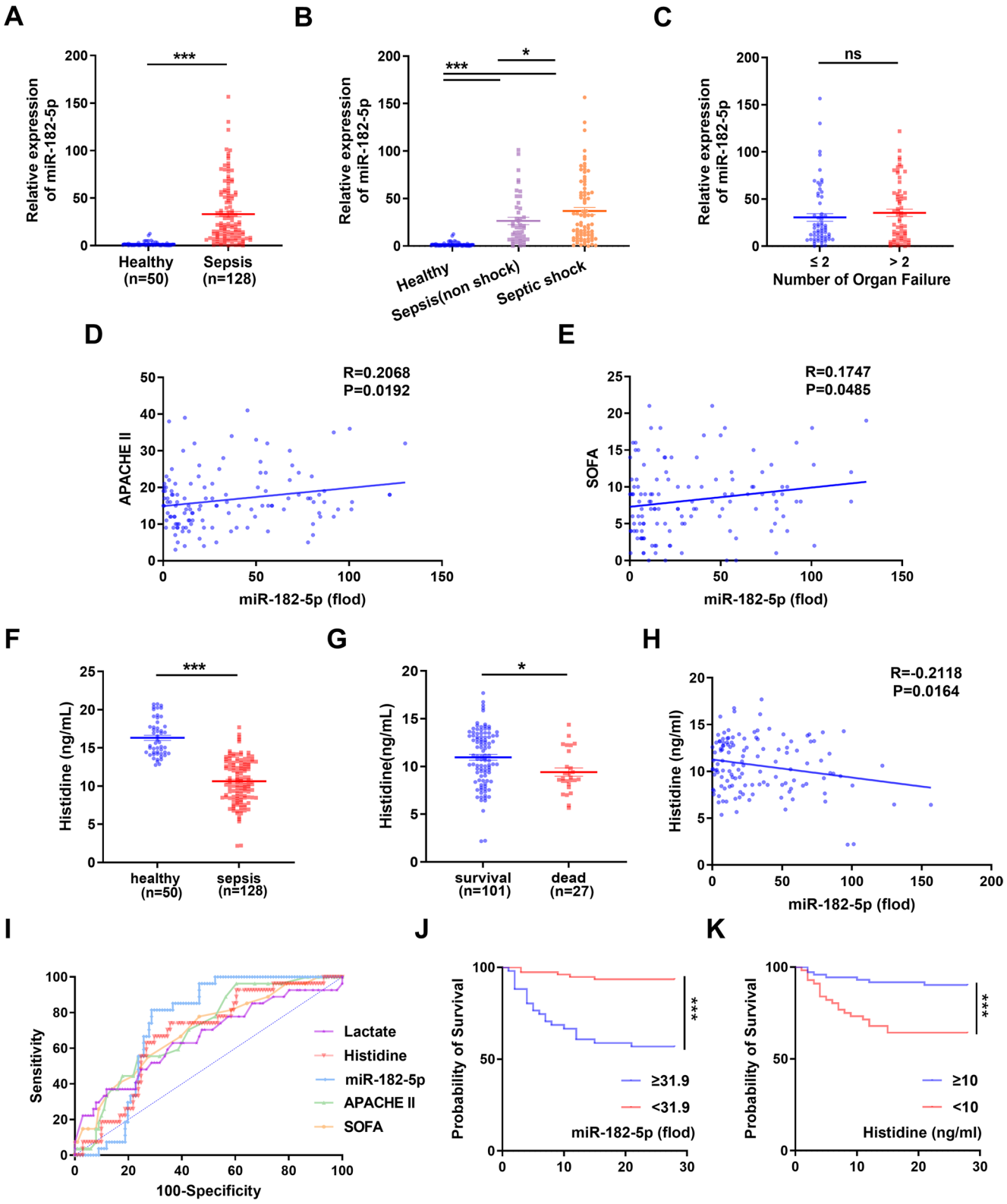

the critical role of miRNAs in maintaining peripheral T cells [43]. In CD4$^+$ T cells, miRNA knockdown promotes Th1 differentiation while inhibiting Th2 and Th17 differentiation [44]. On top of that, miRNAs are pivotal for intra-thymus development as well as peripheral induction of Tregs [45]. Thus, miRNAs are indispensable for the development and differentiation of T cells [46]. miR-182 suppresses IL-2 production by targeting Bach2 and Cd2ap to maintain Treg

Table 2 AUC and cut off for predicting 28-day mortality in septic patients

	Cut off	AUC	Sensitivity (%)	Specificity (%)	*P* value	95% CI
Lactate, mmol/L	3.75	0.657	62.96	63.67	0.0122	0.534–0.781
APACHE II score	12.5	0.702	96.3	39.6	0.0013	0.6024–0.8025
SOFA score	9.5	0.695	55.56	72.28	0.0019	0.5852–0.8042
miR-182, ng/ml	31.9	0.735	81.48	71.29	0.0002	0.651–0.818
Histidine, ng/ml	10	0.676	74.07	64.36	0.0050	0.5717–0.7807

APACHE II acute physiology and chronic health evaluation score, *SOFA* sequential organ failure assessment score, *AUC* area under the curve, *CI* confidence interval

immunosuppression and enhances Treg stability via the IL-4/cMaf axis in Th2-polarized environments, restraining hyperactive immunity while preserving immune tolerance [47]. However, the immunoregulatory functions of miR-182 in septic T cells have not been fully elucidated. Our study observed a significant increase in miR-182 expression in the peripheral blood and spleen of septic mice. This led us to hypothesize that miR-182 may contribute to the immune dysfunction seen in sepsis. Knockout of miR-182 revealed great changes in T cell differentiation. Specifically, the proportion of lymphocytes and $CD4^+$ T cells was found to be increased, while the proportion of Th1, Th2, Th17 and Tregs were significantly reduced compared to the WT group. No significant changes were observed in $CD4^+$ memory T cells, but $CD8^+$ memory T cells underwent conversion into terminally differentiated memory T cells. In vivo, knockout of miR-182 markedly reduced lung and kidney tissue damage, and increased the survival rates post CLP. To sum up, miR-182 had a regulatory effect on T cell differentiation in sepsis, and its knockout may ameliorate the immunosuppression and protect against organ damage in septic mice.

It has been found that miR-182 suppresses T-cell function by inhibiting FOXO1, TCR/CD3 complex, NFATs and IL-2/IL-2RA signaling pathway [48]. miR-182 overexpression inhibits Th17 development and reduces disease severity in experimental autoimmune uveitis by targeting TAF15 and regulating STAT3 pathway [49]. miR-182 overexpression also leads to the promotion of naïve T-cell differentiation towards Th1 and Th17 by targeting HIF-1α and increasing IFN-γ expression [50]. However, the exact mechanism of the regulatory role of miR-182 in sepsis remains unclear. In this study, the combination of metabolomics and proteomics analysis revealed that two differential proteins HAL and ALDH1A1 as well as the differential metabolite 1-methylhistamine were closely related to histidine metabolism. Thus, we speculated miR-182 affected T cell differentiation by regulating histidine metabolism.

FOXO3, as a transcription factor, plays a critical role in regulating cellular homeostasis, stress response, and lifespan. It modulates various stress reactions, including those triggered by nutrient deprivation, oxidative stress, hypoxia, heat shock, and DNA damage [51]. In acute viral infections, FOXO3-deficient mice showed significant expansion of effector $CD8^+$ T cells, with increased memory cell numbers due to reduced apoptosis [52, 53]. In chronic viral infections, FOXO3 contributes to the activation of $CD8^+$ T cells, limiting inflammatory sequelae from the viral infection, and is negatively correlated with the abundance of multifunctional virus-specific cells [54, 55]. Our study demonstrates that miR-182 is an important regulator of FOXO3 expression in sepsis. The regulation of FOXO3 by miR-182 may be one mechanism underlying the altered immune function of T cells in sepsis. Therefore, FOXO3a could be a potential target for immune therapies in both acute and chronic viral infections.

In the present study, we observed reduced histidine levels in sepsis, suggesting its potential role in immune dysregulation. Exogenous histidine administration suppressed Treg proportions and IL-10/TGF-β secretion, possibly through conversion to histamine by histidine decarboxylase (HDC), a known inhibitor of Treg function [56]. However, the precise mechanism linking histamine to Treg suppression in sepsis warrants further exploration.

Clinically, APACHE II and SOFA scores are commonly used to assess the severity of critical illness [57, 58]. This study suggested that elevated miR-182 level and decreased histidine level were associated with poor prognosis in sepsis, and might serve as prognostic biomarkers for sepsis-associated immunosuppression. However, with only 128 clinical cases, further large-scale studies and follow-up data are needed to confirm their clinical value as prognostic biomarkers for sepsis.

Taken together, this study indicates that miR-182 acts as a key regulator of T cell immune paralysis, particularly influencing the distribution of $CD4^+$ and $CD8^+$ T cells, and modulating immune tolerance through Tregs. Mechanistic analysis reveals that knockout of miR-182 decreases the expression of key enzymes of histidine catabolism, affecting T cell function, especially Tregs. Furthermore, our findings suggest that miR-182 might regulate histidine metabolism through targeting FOXO3. In vivo, histidine supplementation attenuates immunosuppression of Tregs in septic mice. Clinically, plasma miR-182 levels in sepsis patients are positively correlated with their severity. These findings may provide new insights to elucidate the molecular pathogenesis of immunosuppressive T cells in sepsis, and guide future pharmacological interventions for sepsis therapy.

Supplementary Information The online version contains supplementary material available at https://doi.org/10.1007/s10753-025-02333-1.

Acknowledgements This study was financially supported by grants from the Natural Science Foundation of Zhejiang Province (LQ22H150003), the Zhejiang Provincial Medical and Health Science and Technology Plan Project (2024KY148), the Traditional Chinese Medicine Technology Project of Zhejiang Province (2024ZL608) and the Wenzhou Science and Technology Bureau Project (Y2023078).

Author Contributions C.L. and L.Z. designed and supervised the study. Z.Y. and L.J. performed the experiments. Z.Y. and L.J. drafted the manuscript. Z.L., W.Y. and W.K. analyzed the data and corrected the manuscript. All authors approved the final manuscript.

Data Availability No datasets were generated or analysed during the current study.

Declarations

Competing interests The authors declare no competing interests.

References

1. Freund, Y. et al. 2017. Prognostic accuracy of Sepsis-3 criteria for In-Hospital mortality among patients with suspected infection presenting to the emergency department. *Jama* 317(3):301–308.
2. Evans, L. et al. 2021. Surviving Sepsis campaign: International guidelines for management of Sepsis and septic shock 2021. *Critical Care Medicine* 49(11):e1063–e1143.
3. Chen, L. et al. 2018. Curcumin attenuates sepsis-induced acute organ dysfunction by preventing inflammation and enhancing the suppressive function of Tregs. *International Immunopharmacology* 61:1–7.
4. Coakley, J. D. et al. 2020. *Innate lymphocyte Th1 and Th17 responses in elderly hospitalised patients with infection and Sepsis*. *Vaccines (Basel)*, 8(2):311.
5. Martin, M. D., V. P. Badovinac, and T. S. Griffith. 2020. CD4 T cell responses and the Sepsis-Induced immunoparalysis state. *Frontiers in Immunology* 11:1364.
6. O'Neill, L. A., F. J. Sheedy, and C. E. McCoy. 2011. MicroRNAs: The fine-tuners of Toll-like receptor signalling. *Nature Reviews Immunology* 11(3):163–175.
7. Drury, R. E., D. O'Connor, and A. J. Pollard. 2017. The clinical application of MicroRNAs in infectious disease. *Frontiers in Immunology* 8:1182.
8. Stittrich, A. B. et al. 2010. The MicroRNA miR-182 is induced by IL-2 and promotes clonal expansion of activated helper T lymphocytes. *Nature Immunology* 11(11):1057–1062.
9. Ojha, R. et al. 2019. Emerging role of Circulating MicroRNA in the diagnosis of human infectious diseases. *Journal of Cellular Physiology* 234(2):1030–1043.
10. Holeček, M. 2020. *Histidine in health and disease: Metabolism, physiological importance, and use as a supplement*. *Nutrients*, 12(3):848.
11. Tan, S. P. et al. 2017. Feeding filaggrin: Effects of l-histidine supplementation in atopic dermatitis. *Clin Cosmet Investig Dermatol* 10:403–411.
12. Hisatsune, T. et al. 2016. Effect of anserine/carnosine supplementation on verbal episodic memory in elderly people. *Journal of Alzheimer'S Disease* 50(1):149–159.
13. DiNicolantonio, J. J., M. F. McCarty, and O. K. JH. 2018. Role of dietary histidine in the prevention of obesity and metabolic syndrome. *Open Heart* 5(2):e000676.
14. Rittirsch, D., M. S. Huber-Lang, M. A. Flierl, and P. A. Ward. 2009. Immunodesign of experimental sepsis by cecal ligation and puncture. *Nature Protocols* 4(1):31–36.
15. Becht, E. et al. 2018. *Dimensionality reduction for visualizing single-cell data using UMAP*. Nat Biotechnol.
16. Pauken, K. E., and E. J. Wherry. 2015. SnapShot: T cell exhaustion. *Cell* 163(4):1038–1038e1.
17. Xu, J. et al. 2021. Lactate up-regulates the expression of PD-L1 in kidney and causes immunosuppression in septic acute renal injury. *Journal of Microbiology, Immunology, and Infection* 54(3):404–410.
18. Jensen, I. J., F. V. Sjaastad, T. S. Griffith, and V. P. Badovinac. 2018. Sepsis-Induced T cell immunoparalysis: The Ins and outs of impaired T cell immunity. *The Journal of Immunology* 200(5):1543–1553.
19. Fernández-Grande, E. et al. 2019. Enhanced HLA-DR expression on T-lymphocytes from patients in early stages of non-surgical sepsis. *Med Clin (Barc)* 152(9):346–349.
20. Shevach, E. M. 2009. Mechanisms of foxp3+T regulatory cell-mediated suppression. *Immunity* 30(5):636–645.
21. Ottens, K. et al. 2018. Foxo3 promotes apoptosis of B cell receptor-Stimulated immature B cells, thus limiting the window for receptor editing. *The Journal of Immunology* 201(3):940–949.
22. Haoues, M. et al. 2014. Forkhead box O3 (FOXO3) transcription factor mediates apoptosis in BCG-infected macrophages. *Cellular Microbiology* 16(9):1378–1390.
23. Togher, S., A. Larange, S. P. Schoenberger, and S. Feau. 2015. FoxO3 is a negative regulator of primary CD8+T-cell expansion but not of memory formation. *Immunology and Cell Biology* 93(2):120–125.
24. Pepper, M., and M. K. Jenkins. 2011. Origins of CD4(+) effector and central memory T cells. *Nature Immunology* 12(6):467–471.
25. Ying, L. et al. 2017. *Mitofusin 2 Promotes Apoptosis of CD4(+) T Cells by Inhibiting Autophagy in Sepsis*. Mediators Inflamm, 2017 4926205.
26. Taylor, M. D. et al. 2020. CD4 and CD8 T cell memory interactions alter innate immunity and organ injury in the CLP Sepsis model. *Frontiers in Immunology* 11:563402.
27. Ye, Q., W. X. Shao, Q. Q. Wang, and J. H. Mao. 2019. An imbalance of T cell subgroups exists in children with sepsis. *Microbes and Infection* 21(8–9):386–392.
28. Kong, B. et al. 2018. Effects of Simvastatin on the function of Splenic CD4(+) and CD8(+) T cells in sepsis mice. *Immunologic Research* 66(3):355–366.

29. Li, G. et al. 2020. Increased Th17 and Th22 cell percentages predict acute lung injury in patients with Sepsis. *Lung* 198(4):687–693.
30. Gupta, D. L. et al. 2016. Coexistence of Th1/Th2 and Th17/Treg imbalances in patients with post traumatic sepsis. *Cytokine* 88:214–221.
31. Venet, F. et al. 2006. Human CD4+CD25+regulatory T lymphocytes inhibit lipopolysaccharide-induced monocyte survival through a fas/fas ligand-dependent mechanism. *The Journal of Immunology* 177(9):6540–6547.
32. Lewkowicz, P., N. Lewkowicz, A. Sasiak, and H. Tchórzewski. 2006. Lipopolysaccharide-activated CD4+CD25+T regulatory cells inhibit neutrophil function and promote their apoptosis and death. *The Journal of Immunology* 177(10):7155–7163.
33. Venet, F. et al. 2009. Increased Circulating regulatory T cells (CD4(+)CD25 (+)CD127 (-)) contribute to lymphocyte anergy in septic shock patients. *Intensive Care Medicine* 35(4):678–686.
34. Ioanna, Z., B. Katerina, and A. Irene. 2021. Immunotherapy-on-Chip against an experimental Sepsis model. *Inflammation* 44(6):2333–2345.
35. Chen, W. et al. 2017. Ethyl pyruvate reverses development of Pseudomonas aeruginosa pneumonia during sepsis-induced immunosuppression. *International Immunopharmacology* 52:61–69.
36. Liu, P. et al. 2020. Baicalin suppresses Th1 and Th17 responses and promotes Treg response to ameliorate sepsis-associated pancreatic injury via the RhoA-ROCK pathway. *International Immunopharmacology* 86:106685.
37. Qiu, D. et al. 2019. Gpr174-deficient regulatory T cells decrease cytokine storm in septic mice. *Cell Death and Disease* 10(3):233.
38. Henning, A. N., R. Roychoudhuri, and N. P. Restifo. 2018. Epigenetic control of CD8(+) T cell differentiation. *Nature Reviews Immunology* 18(5):340–356.
39. Kurachi, M. 2019. CD8(+) T cell exhaustion. *Seminars in Immunopathology* 41(3):327–337.
40. Xiao, C., and K. Rajewsky. 2009. MicroRNA control in the immune system: Basic principles. *Cell* 136(1):26–36.
41. Cobb, B. S. et al. 2005. T cell lineage choice and differentiation in the absence of the RNase III enzyme Dicer. *Journal of Experimental Medicine* 201(9):1367–1373.
42. Chong, M. M. et al. 2010. Canonical and alternate functions of the MicroRNA biogenesis machinery. *Genes & Development* 24(17):1951–1960.
43. Muljo, S. A. et al. 2005. Aberrant T cell differentiation in the absence of Dicer. *Journal of Experimental Medicine* 202(2):261–269.
44. Ichiyama, K. et al. 2016. The MicroRNA-183-96-182 cluster promotes T helper 17 cell pathogenicity by negatively regulating transcription factor Foxo1 expression. *Immunity* 44(6):1284–1298.
45. Baumjohann, D. et al. 2013. The MicroRNA cluster miR-17∼92 promotes TFH cell differentiation and represses subset-inappropriate gene expression. *Nature Immunology* 14(8):840–848.
46. Baumjohann, D., and K. M. Ansel. 2013. MicroRNA-mediated regulation of T helper cell differentiation and plasticity. *Nature Reviews Immunology* 13(9):666–678.
47. Kelada, S. et al. 2013. miR-182 and miR-10a are key regulators of Treg specialisation and stability during schistosome and Leishmania-associated inflammation. *Plos Pathogens* 9(6):e1003451.
48. Soheilifar, M. H. et al. 2021. Concomitant overexpression of mir-182-5p and mir-182-3p raises the possibility of IL-17-producing Treg formation in breast cancer by targeting CD3d, ITK, FOXO1, and nfats: A meta-analysis and experimental study. *Cancer Science* 112(2):589–603.
49. Zhang, L. et al. 2020. miR-182-5p inhibits the pathogenic Th17 response in experimental autoimmune uveitis mice via suppressing TAF15. *Biochemical and Biophysical Research Communications* 529(3):784–792.
50. Wang, M. et al. 2019. Knockdown of LncRNA ZFAS1 inhibits progression of nasopharyngeal carcinoma by sponging miR-135a. *Neoplasma* 66(6):939–945.
51. Bernardo, V.S., F.F. Torres, and D.G.H. da Silva. 2023. FoxO3 and oxidative stress: a multifaceted role in cellular adaptation. *Journal of MolecularMedicine (Berl)* 101 (1–2): 83–99.
52. Sullivan, J. A. et al. 2012. FOXO3 regulates CD8 T cell memory by T cell-intrinsic mechanisms. *Plos Pathogens* 8(2):e1002533.
53. Tzelepis, F. et al. 2013. Intrinsic role of FoxO3a in the development of CD8+T cell memory. *The Journal of Immunology* 190(3):1066–1075.
54. Zhang, X., et al. 2017. FOXO3, IRF4, and xIAP Are Correlated with Immune Activation in HIV-1-Infected Men Who Have Sex with Men During Early HIV Infection. *AIDS Research and Hum an Retroviruses* 33 (2): 172–180.
55. Litvak, V. et al. 2012. A FOXO3-IRF7 gene regulatory circuit limits inflammatory sequelae of antiviral responses. *Nature* 490(7420):421–425.
56. Tamaka, K. et al. 2015. Histamine suppresses regulatory T cells mediated by TGF-β in murine chronic allergic contact dermatitis. *Experimental Dermatology* 24(4):280–284.
57. Dosi, R. et al. 2021. The predictive ability of SAPS II, APACHE II, SAPS III, and APACHE IV to assess outcome and duration of mechanical ventilation in respiratory intensive care unit. *Lung India* 38(3):236–240.
58. Niknam, K. et al. 2021. EccSOFA: SOFA illness severity score adapted to predict in-hospital mortality in emergency critical care patients. *American Journal of Emergency Medicine* 41:145–151.